

EJECTION OF SUPERNOVA-ENRICHED GAS FROM DWARF DISK GALAXIES

P. CHRIS FRAGILE, STEPHEN D. MURRAY

University of California, Lawrence Livermore National Laboratory, P.O. Box 808, Livermore, CA 94550

AND

DOUGLAS N. C. LIN

University of California, Lick Observatory, Santa Cruz, CA 95064

Draft version November 23, 2018

ABSTRACT

We examine the efficiency with which supernova-enriched gas may be ejected from dwarf disk galaxies, using a methodology previously employed to study the self-enrichment efficiency of dwarf spheroidal systems. Unlike previous studies that focused on highly concentrated starbursts, in the current work we consider discrete supernova events spread throughout various fractions of the disk. We model disk systems having gas masses of 10^8 and $10^9 M_{\odot}$ with supernova rates of 30, 300, and 3000 Myr^{-1} . The supernova events are confined to the midplane of the disk, but distributed over radii of 0, 30, and 80% of the disk radius, consistent with expectations for Type II supernovae. In agreement with earlier studies, we find that the enriched material from supernovae is largely lost when the supernovae are concentrated near the nucleus, as expected for a starburst event. In contrast, however, we find the loss of enriched material to be much less efficient when the supernovae occur over even a relatively small fraction of the disk. The difference is due to the ability of the system to relax following supernova events that occur over more extended regions. Larger physical separations also reduce the likelihood of supernovae going off within low-density “chimneys” swept out by previous supernovae. We also find that, for the most distributed systems, significant metal loss is more likely to be accompanied by significant mass loss. A comparison with theoretical predications indicates that, when undergoing self-regulated star formation, galaxies in the mass range considered shall efficiently retain the products of Type II supernovae.

Subject headings: galaxies: dwarf — galaxies: evolution — hydrodynamics — methods: numerical — supernovae: general — galaxies: abundances

1. INTRODUCTION

In cosmological models dominated by cold dark matter (CDM), the amplitude of fluctuations increases toward shorter wavelengths. Small galaxies are therefore the first to form, and large galaxies subsequently form through the merger of smaller systems (e.g. White & Rees 1978; Blumenthal et al. 1984; Cole et al. 1994; Klypin, Nolthenius, & Primack 1997; Navarro, Frenk & White 1997). The very first generations of star formation, and hence the initial enrichment of the interstellar and intergalactic medium, therefore likely occurred within dwarf galaxies. Much recent attention has been paid to understanding the gas evolution and first generations of stars within such systems (e.g. Dekel & Silk 1986; Katz et al. 1996; Quinn, Katz, & Efstathiou 1986; Tegmark et al. 1987; Weinberg, Hernquist, & Katz 1997; Mac Low & Ferrara 1999; Sommer-Larsen, Gelato, & Vedel 1999; Sommer-Larsen, Götz, & Portinari 2003; Fragile et al. 2003).

Observational work is also shedding light upon the early evolution of dwarf galaxies. Because the comoving density of damped Ly α systems (DLAs) at $z > 2$ is comparable to that of all the ordinary matter in galactic disks today, it is tempting to identify the DLAs as the objects that evolved into the present-day L $_{\ast}$ galaxies (Kauffmann 1996). The observationally inferred star-formation rates per unit surface area in such systems are similar to that in the Milky Way today (Wolfe, Prochaska, & Gawiser 2003). Recent observations find that the DLA metallicity evolves significantly with redshift. The overall metallicities are,

however, well below that expected from observationally inferred star-formation rates, implying a significant loss rate of enriched gas from these systems (Prochaska et al. 2003).

In addition to governing the early enrichment of the universe, star formation within dwarf systems affects their dynamical evolution as they merge to form more massive galaxies. One important issue is the “angular momentum problem.” In CDM models which include only cooling, the first objects to form rapidly cool and contract. Numerical simulations show a tendency for dwarf galaxy building blocks to undergo dynamical friction and to lose a large fraction of their initial angular momentum prior to merging, leading to the formation of massive galaxies that are much more compact and have much less angular momentum than observed (Sommer-Larsen, Gelato, & Vedel 1999). Some cosmological models have avoided this problem by invoking *ad hoc* star-formation rates within dwarf systems, in order to heat their gas and maintain large radii.

In earlier work, we have explored star formation that is self-consistently governed by negative feedback, in a self-regulating process. That picture has had good success in matching the star-formation rates seen in spheroids and disks (Lin & Murray 1999, 2000), and in matching observational data for dwarf spheroidal systems (dSphs) (Dong, Lin, & Murray 2003).

For dSphs, Dong, Lin, & Murray (2003) find that star formation may occur in bursts. In such low mass systems,

even a small burst of supernovae can lead to a substantial loss of enriched gas (Fragile et al. 2003). In more massive dwarf disk galaxies, however, where the dynamical times exceed the characteristic timescales for star formation and feedback effects, star formation is expected, in the absence of dynamical interactions between galaxies, to be a much more steady-state process.

The ejection of enriched gas from dwarf disk systems has been examined in many previous studies (De Young & Gallagher 1990, 1994; Silich & Tenorio-Tagle 1998; Mac Low & Ferrara 1999; Sommer-Larsen, Götz, & Portinari 2003). In those studies, it was found that the efficiency with which enriched material is ejected from dwarf disk galaxies may be quite high. Even in systems with gas masses as high as $10^9 M_\odot$ ($10^{10} M_\odot$ total mass), the ejection efficiency of enriched material was 97% for a supernova rate of one per 30,000 yr (Mac Low & Ferrara 1999). This efficiency is especially striking given that, measured per unit gas mass, the supernova rates assumed are more than two orders of magnitude below that of the Milky Way today. The high ejection efficiency in the modeled dwarf systems is the result of both the shallower potential of the lower mass galaxy and the mode of star formation. In Mac Low & Ferrara (1999), the supernova energy was input as a continuous luminosity source at the center of the model galaxies, and so the systems were unable to relax between discrete supernova events. Sommer-Larsen, Götz, & Portinari (2003) allowed star formation to occur with high local efficiency whenever the gas density exceeded a critical value, resulting in strong bursts of star formation that also led to efficient ejection of enriched gas. These models, therefore, best represent the evolution of concentrated starbursts within the dwarf disk systems and indicate that even mild starbursts may lead to significant loss of enriched material.

In general, however, star formation is not limited to concentrated regions within young galaxies. Although it is expected to occur most strongly within regions of higher gas surface density, it shall occur throughout the disk, as is supported both by observational data (Gallagher & Hunter 1987; Kennicutt 1989) and self-regulating models (Lin & Murray 1999). Because self-regulating star formation is expected to dominate the life history of galaxies, it is of interest to see how efficiently the enriched material produced by this more quiescent process is retained.

We note here that our simulations restrict supernovae to occur in the regions of our models where the gas density is greatest, namely the midplanes. As we discuss below, this is consistent with expectations for Type II supernovae, since they occur mostly in regions of high star formation efficiency. Type I supernovae, on the other hand, which are believed to be responsible for most of the iron production within galaxies, come from older objects, which may have migrated significantly from their birthplaces and so may occur at heights well above the disk plane. In a follow up paper, we will consider the impact of Type I supernovae and the implication on the contamination of clusters of galaxies.

In this paper, we extend our earlier work on the ejection of enriched gas from dSphs (Fragile et al. 2003), by examining three-dimensional simulations of supernova energy input to dwarf disk galaxies, in which the supernovae

occur as discrete events, spread out over significant fractions of the disk. We describe our numerical method and the setup of the models in § 2. The results of the models are discussed in § 3, and conclusions for the evolution of dwarf disk systems are discussed in § 4.

2. NUMERICAL METHOD

2.1. Numerical Code

The models discussed below have been computed using Cosmos, a massively parallel, multidimensional, radiation-chemo-magneto-hydrodynamics code for both Newtonian and relativistic flows developed at Lawrence Livermore National Laboratory. Tests of the Newtonian hydrodynamics options and of the internal physics relevant to the current work are presented in Anninos, Fragile & Murray (2003) and shall not be discussed in detail here.

Because we shall be examining the effects of having multiple supernova explosions at random locations throughout the cores of dwarf galaxies, our models are run in three-dimensions on a Cartesian mesh. The simulations are run on a $256 \times 256 \times 128$ grid with a physical box size of $30 \text{ kpc} \times 30 \text{ kpc} \times 15 \text{ kpc}$. Each zone, therefore, measures 117 pc on a side. We explore the impact of numerical resolution on our results by also performing one simulation at a resolution of $128 \times 128 \times 64$. We use flat (zero-gradient) boundary conditions at each of the outer boundaries and a reflective boundary along the midplane of the disk. Because highly evacuated regions can be a problem for numerical hydrodynamics codes, we maintain a strict density floor at 10^{-5} of the initial midplane density of the galaxy.

The code parameters used for the present work are similar to those used previously in studying the evolution of enriched material in dwarf spheroidal galaxies (Fragile et al. 2003) and in jet-cloud interactions (Fragile et al. 2004). Chemistry is not followed in these simulations, and cooling is given by an equilibrium cooling function, assuming low metallicity ($Z = 0.03Z_\odot$). In order to simulate the effects of equilibrium heating, cooling is suppressed below 10^4 K . Due to our inability to resolve the cooling regions behind shocks, cooling is also restricted whenever $Q/P > 0.1$, where Q is the scalar artificial viscosity and P is the thermal gas pressure. This should help prevent overcooling in the unresolved post-shock gas, although this was not found to have a strong effect upon the evolution of dwarf spheroidal galaxy models (Fragile et al. 2003).

2.2. Galaxy Model

The galaxies are modeled as non-self gravitating gas within a fixed dark-matter (DM) potential. The omission of self-gravity is reasonable, given that the baryonic-to-dark matter ratio of the systems is ~ 0.1 . In order to facilitate comparisons with previous work, we adopt the same form for the galactic potential as used by both Mac Low & Ferrara (1999) and Silich & Tenorio-Tagle (2001). The spheroidal DM mass distribution is given by

$$\rho_d(r) = \frac{\rho_c}{1 - (r/R_c)^2}, \quad (1)$$

where the central density (ρ_c) and scale radius (R_c) are (Silich & Tenorio-Tagle 2001)

$$\rho_c = 6.3 \times 10^{10} \left(\frac{M_d}{M_\odot} \right)^{-1/3} h^{-1/3} M_\odot \text{ kpc}^{-3} \quad (2)$$

$$R_c = 8.8 \times 10^{-6} \left(\frac{M_d}{M_\odot} \right)^{1/2} h^{1/2} \text{ kpc} , \quad (3)$$

where M_d is the mass of the dark matter halo and h is the Hubble constant in units of $100 \text{ km s}^{-1} \text{ Mpc}^{-1}$. We adopt $h = 0.65$, consistent with measurements using Type Ia supernovae (Gibson, Maloney & Sakai 2000) and gravitational lensing (Williams & Saha 2000), and slightly smaller than the value determined by recent Cepheid measurements (Freedman et al. 2001). The tidal radius of the dark matter halo (R_t) is given by (Mac Low & Ferrara 1999):

$$R_t = 0.016 \left(\frac{M_d}{M_\odot} \right)^{1/3} h^{-2/3} \text{ kpc} . \quad (4)$$

The total mass of the halo is

$$M_d = 4\pi \int_0^{R_t} \rho_d(r) r^2 dr = 4\pi \rho_c R_c^3 (x_t - \arctan x_t) , \quad (5)$$

where $x_t = R_t/R_c$, is related to the mass of the visible (gas plus stellar) matter (M_g) by (Persic, Salucci, & Stel 1996)

$$\frac{M_d}{M_g} \simeq 34.7 \left(\frac{M_g}{10^7 M_\odot} \right)^{-0.29} . \quad (6)$$

The gravitational potential of the halo is

$$\phi(r) = 4\pi G \rho_c R_c^2 \left[\frac{1}{2} \ln(1+x^2) + \frac{\arctan x}{x} \right] , \quad (7)$$

where $x = r/R_c$. The interstellar gas density is then distributed according to (Silich & Tenorio-Tagle 1998)

$$\rho = \rho_0 \exp \left[\frac{3}{2} \left(\frac{V_{esc}}{c_s} \right)^2 \chi \right] , \quad (8)$$

where ρ_0 is the gas density at the galactic center and $V_{esc} = (2GM_d/R_t)^{1/2}$ is the escape velocity at the halo boundary (R_t). We adopted the equation of state of an ideal gas with cooling and heating such that the effective sound speed evolves with time. Here c_s is the initial value of the sound speed. The function χ determines the density distribution in the (vertical) direction normal to the disk. It has the form (Silich & Tenorio-Tagle 1998)

$$\chi = F(r) - F(\varrho) , \quad (9)$$

where ϱ is the cylindrical radius and

$$F(r) = 1 + \frac{4\pi\rho_c R_c^3}{M_d} x_t \left\{ \frac{1}{2} [\ln(1+x_t^2) - \ln(1+x^2)] + \frac{\arctan x_t}{x_t} - \frac{\arctan x}{x} \right\} . \quad (10)$$

The gas disk extends out to a cutoff radius, which depends upon the gas mass following the relation (Ferrara & Tolstoy 2000)

$$R_d = 3 \left(\frac{M_g}{10^7 M_\odot} \right)^{0.338} \text{ kpc} . \quad (11)$$

Vertically, the disk extends to a height determined by $P = P_{IGM}$, where $P = \rho c_s^2$ is the interstellar gas pressure.

The value of ρ_0 in equation 8, which sets the midplane density, is scaled to give the desired gas mass M_g within R_d . This density distribution is chosen primarily for the purpose of comparison with other calculations. Although it does not represent that of an exponential disk, the gas profile is a reasonable approximation to dwarf galaxies. In the midplane of the galaxy, the gas is supported radially against gravity entirely by rotation. The circular velocity of the galaxy is

$$v_c^2(r) = r \frac{\partial \phi}{\partial r} = \frac{4\pi G \rho_c R_c^2}{x} (x - \arctan x) . \quad (12)$$

Our models are, therefore, completely specified by choosing M_g , c_s , and P_{IGM} . In this work, all models use $c_s = 10 \text{ km s}^{-1}$ and $P_{IGM}/k = 1 \text{ cm}^{-3} \text{ K}$. In Models 1-7, we choose $M_g = 10^9 M_\odot$, which corresponds to $M_d \sim 10^{10} M_\odot$, $v_c \sim 35 \text{ km s}^{-1}$, $R_c \sim 1 \text{ kpc}$, $R_d \sim 14 \text{ kpc}$, and $R_t \sim 30 \text{ kpc}$. The gas mass in Model 8 is an order of magnitude smaller. The masses of these models are smaller than L_* galaxies but much larger than dwarf spheroidals.

2.3. Supernova Input

In this work supernova events are simulated by adding either 10^{51} or 10^{52} erg of internal energy to the gas over finite regions; other fluid variables remain unchanged. The internal energy is injected over an approximately spherical volume with a ‘‘top-hat’’ profile of 1-4 zones radius. Normally a radius of 2 zones is used, yielding an initial supernova gas temperature of $T_{SN} \gtrsim 10^6 \text{ K}$ for a 10^{52} erg event. For the low metallicities used in these simulations, this lies close to the minimum of the cooling function, helping prevent the supernova gas from cooling too quickly. A supernova radius of 1 zone is used for our low-resolution ($128 \times 128 \times 64$) simulation, in order to keep the size of the input region as similar as possible to the higher resolution equivalent. We only use a supernova radius of 4 zones for the highest luminosity model considered (Model 7). Although supernova events at the beginning of that simulation may cool too rapidly, the high event rate ensures that later supernovae are set off in previously evacuated regions and are not subject to excessive cooling.

Whenever supernova events are set off, a passive tracer is added to the same zones to which the energy is initially added. We use this tracer to track the ejection of enriched material as described in §2.5.

Runs with supernova events of 10^{52} erg increase the chances of a single event successfully expelling enriched material from the galaxy. This also helps ensure that a reasonable minimum floor temperature is maintained for the supernovae ($T_{SN} \gtrsim 10^6 \text{ K}$). This treatment simulates the fact that multiple supernovae are often expected to occur in localized regions, centered upon OB associations. The effective local energy input in these regions is therefore expected to exceed that of a single supernova. However, the more energetic events can be computationally expensive to evolve for a time-explicit code such as Cosmos, especially when supernova events overlap, as occurs in either our most confined runs or highest luminosity cases. Therefore, some runs input 10^{51} erg per event. For these runs most of the supernovae go off in previously evacuated regions so they have a relatively high initial temperature, although some of the early supernovae may be much cooler.

To illustrate some of the properties of these supernova events, we first simulate a single event in a homogeneous background. This simulation uses the same grid spacing as our standard models (117 pc). Gravity is not considered and the background is set to a uniform density and temperature equal to the initial midplane values of our $10^9 M_\odot$ galaxy. We evolve the model for 100 Myr, the same as most of our galaxy models. In Figure 1, we plot several fluid variables as a function of radius at equally spaced intervals of time. Here we comment on a few key observations from that simulation. First, it is apparent that much of the cooling of the supernova gas is dominated by adiabatic expansion, although some radiative cooling does take place in the dense post-shock shell. Also, the supernova expansion closely follows the Sedov-Taylor solution. This is best illustrated in Figure 2, which shows the radius of the shock front (r_{sh}) as a function of time. The data are best fit with a power-law of the form $r_{sh} \propto t^{0.41}$, very close to the Sedov-Taylor solution $r_{sh} \propto t^{2/5}$. One concern, however, is the noticeable mixing of tracer material in the post-shock shell (lower right panel of Figure 1). Although, some mixing is expected due to hydrodynamic (Rayleigh-Taylor and Kelvin-Helmholtz) instabilities, there is also the possibility of anomalous mixing due to numerical diffusion. Since the tracer is a surrogate for enriched gas mass in these simulations, this suggests that the metal ejection efficiency could be artificially reduced due to excessive mixing of cold, “heavy” background gas with the supernova gas. This is one motivation for testing our results at a different resolution, since this will provide some indication of how problematic numerical diffusion is. We also point out that, by $t \gtrsim 10$ Myr or an expansion radius of $r_{sh} \gtrsim 800$ pc, the post-shock gas in the supernova is already traveling slower than the local escape speed at the core of our galaxy models. This is certainly consistent with our findings that a single supernova event (even a 10^{52} erg event) is not sufficient to eject enriched material from the galaxy potentials studied here [nor was a single 10^{51} erg event sufficient for the much smaller dwarf spheroidal galaxies studied in Fragile et al. (2003)]. Multiple overlapping events or pre-existing voids are crucial to propelling the enriched material out of the galaxy.

In the remaining simulations, the supernova events are distributed randomly in space and time, subject to the following restrictions: the average rate of events is a fixed parameter within each model; all supernovae are restricted to the midplane of the galaxy; and supernovae are restricted to lie within a specified radius of the galactic center, with their distribution weighted by the enclosed area. Confining supernova events to the midplane makes it more reasonable to employ a reflective boundary as we have done. This also maximizes the probability that the galaxy will be able to contain the energy of each event and retain the enriched material. Because star formation is expected to be strongly concentrated where the gas density is greatest, limiting supernova events to the midplane is also a reasonable approximation to their actual distribution (at least for Type II supernovae).

2.4. Model Parameters

The parameters of the models are listed in Table 1. For each model, we list the gas mass of the galaxy (M_g), the energy input rate, the energy per supernova event, the

fractional radius of the disk over which the supernovae occur (R_{SN}/R_d), the time interval over which the supernovae are initialized, and the total simulation time.

The parameters for Model 1 are selected so as to closely match the highest mass, highest luminosity model of Mac Low & Ferrara (1999). The primary difference is that the supernovae occur discretely in time, as is the case in all our models. In order to more closely match the results of Mac Low & Ferrara (1999), who use a continuous input of energy, the supernova events in Model 1 have 10^{51} erg each. The high supernova frequency helps to ensure that the nuclear gas does not have substantial time to relax between events, which should help to minimize the differences between this model and the earlier work. The duration of supernovae input phase is set by two factors. The main sequence lifetime of the smallest stars that become supernovae is 50 Myr (Stothers 1972; McCray & Kafatos 1987). This sets the minimum timespan over which supernovae shall occur, in the limit of an instantaneous burst of star formation. The timespan shall be larger if star formation occurs over an extended time period. One characteristic timescale is the dynamical time of the core, ~ 30 Myr for Model 1. The total timescale over which supernovae may occur could therefore be close to 100 Myr. We adopt the minimum time scale for Model 1, and note that had we injected the same supernova energy over the longer timescale, the loss of enriched gas might be reduced from that found in Model 1.

Models 2-7 use the same unperturbed system as Model 1. Model 2 is exactly the same as Model 1 except that the supernovae are all set off at a single point half-way out in the disk. The scale height of the gas increases with radius, and so this model examines the ability of a non-nuclear starburst to expel enriched material, given that it must work its way through a larger volume of interstellar gas. Models 3 and 4 use the same energy input rate as Model 1 but with ten times more energy per event. In Model 3, the supernova events are spread out over 80% of the galactic disk. Thus, Model 3 represents the opposite extreme of supernova distribution. Because this model is perhaps most sensitive to overcooling and “weighting down” of the enriched material due to the relatively high mass contained in the supernovae (since few go off inside previously evacuated regions), we also test a version of this model (Model 3b) that enforces a maximum gas density for all the supernova events ($\rho_{SN} < 10^{-26}$ g cm $^{-3}$). If a supernova region exceeds this density ceiling after applying the usual input mechanism, the gas density inside this region is uniformly reduced until this criterion is satisfied. Any gas thus removed from the supernova region is redistributed into a shell of 2 zones thickness around the supernova so as to conserve mass. This technique is effectively equivalent to requiring that all supernovae go off inside evacuated regions and should reduce any overcooling or weighting down of the supernova. Furthermore, since Model 3 is probably more sensitive to resolution effects than any other, we also use this model to test a lower resolution ($128 \times 128 \times 64$) simulation (Model 3c). Model 4 is an intermediate case between Models 1 and 3 with the supernovae spread over 30% of the disk. We consider a longer duration (100 Myr) for the supernovae input phase in Models 3 and 4 to take into account the longer dy-

namical timescale and greater physical distribution of the supernovae sites.

The supernova rate in Models 1-4 (30 Myr^{-1}) is significantly smaller than the presently observed supernova rate in the Milky Way (10^4 Myr^{-1}). However, since the gas disks in these models are comparable in area to that of the Milky Way and have average surface density only about a factor of 3 smaller, one might expect a more comparable supernova rate, perhaps within a factor of 10 (Kennicutt 1998). Models 5 and 6, therefore, are similar to Models 1 and 3, except that the energy input rate is increased by an order of magnitude. In Model 7 the energy input rate is increased by yet another order of magnitude. In Model 8 the mass of the system is reduced by an order of magnitude; otherwise this model is similar to Model 3 with an energy input rate equivalent to 30 supernovae per Myr spread out over 80% of the disk. This model allows us to examine the dependence of the loss of enriched material upon galaxy mass.

In Figure 3, we plot the square root of the absolute value of the normalized gravitational potential ($|\phi - \phi_t|^{1/2}$) as a function of radius for the two galaxy masses considered. This function gives a good estimate of the local escape velocity. At the end of each simulation we use this to estimate the amounts of unenriched and enriched gas that will ultimately escape the galaxy, as described in the next section. We also plot the integrated column density ($\Sigma = \int \rho dz$) as a function of radius in the midplane of the disk. This shows that the flaring of the disk requires that supernovae going of a larger radii must push through a higher column density of material than supernovae occurring near the core. This has a noticeable effect on our results.

2.5. Loss of Enriched Material

We estimate the ejection efficiencies of galactic gas and supernova-enriched material by quantifying how much of each material is traveling faster than the local escape speed of the dark matter halo at the end of the simulation. In this way, we define the mass-ejection efficiency as (Mac Low & Ferrara 1999)

$$\xi = (M_{g,esc} + M_{g,lost})/M_{g,i} , \quad (13)$$

where $M_{g,esc}$ is the gas mass on the grid moving at speeds greater than the escape speed, $M_{g,lost}$ is an estimate of the gas mass lost from the grid at greater than the escape speed, and $M_{g,i}$ is the initial gas mass of the galaxy. Similarly, we define the metal-ejection efficiency as

$$\xi_Z = (\mathcal{T}_{esc} + \mathcal{T}_{lost})/\mathcal{T}_{SN} , \quad (14)$$

where \mathcal{T}_{SN} is the sum of the tracer injected into each simulation and \mathcal{T}_{esc} and \mathcal{T}_{lost} are defined analogously to $M_{g,esc}$ and $M_{g,lost}$. Because our galaxies are not in initial pressure balance at the disk edge, they tend to expand sideways at the sound speed during the course of the simulations. Furthermore, since the larger galaxy models (Models 1-7) initially fill up a large fraction of the grid, they tend to lose gas off of the grid due solely to this sideways expansion. We do not include this loss in our estimate of $M_{g,lost}$. We evaluate ξ and ξ_Z at the end of each run (50, 75, or 100 Myr) and report the results in Table 2.

3. RESULTS

3.1. Model 1

The density and tracer evolution for Model 1 are shown in Figure 4. In this figure, the density distribution of ordinary gas is illustrated using volume visualization. Simultaneously we plot, in red, an isosurface of the tracer gas set at 10^{-3} of the input level. Similar figures are presented for each of our models.

As can be seen in Figure 4, the supernova energy input in Model 1 causes a rapid ‘‘chimneying’’ up the symmetry axis of the galaxy. The preferential motion of enriched gas along the rotation axis leads to a substantial loss. The time history of this loss is presented in Figure 5, alongside data from our other models. This figure tracks the cumulative amount of tracer material inside of R_d for each model as a function of time. Each model is adjusted to the same slope and the results of the models are offset from each other for clarity. The thin solid lines show the adjusted average input rate for each model. Although this plot is useful for illustration, it does not account for enriched material that is traveling faster than the escape speed but still located within R_d . Such material is expected to eventually escape the galactic potential. We will return to this point below.

In Figure 6 we plot, for each of our models, the time history of the total gas mass contained within R_d , normalized to the initial mass of each galaxy. Note that some mass is lost beyond R_d in all models due simply to the fact that these galaxies are not initially in pressure equilibrium at the disk edge. The initial non-equilibrium leads to a fractional mass loss that is identical for Models 1-6, and which has nothing to do with ejection by supernovae. Only Models 7 and 8 show significantly higher mass loss than the more quiescent models. Comparing with Figure 5, we see that enriched material is preferentially lost in nearly all of these models.

While Figures 5 and 6 give a qualitative feel for the ejection history of enriched material and gas mass within our models, the ejection efficiencies defined in §2.5 give a much more physically motivated estimate. The results for each model are summarized in Table 2. For Model 1, although the ejection of enriched material is highly efficient ($\xi_Z = 0.91$), very little mass is lost from the galaxy as a whole ($\xi = 0.023$). We find this to be true for most of our models.

We note that our results for Model 1 are similar, although not identical, to those of Mac Low & Ferrara (1999). This is not unexpected, however, given that the current study uses somewhat lower resolution and a different cooling function. The fundamental conclusion, however, that highly concentrated supernovae trigger substantial loss of enriched material, remains unchanged.

3.2. Model 2

Model 2 is identical to Model 1 except that the supernovae are all initiated at a fixed point half way out in the disk. This allows us to test the dependence of our results on the location of a starburst. In Figure 7 we plot the evolution of the density and tracer for this model; it is obvious that there are significant differences from the results of Model 1. Due to the flaring of the galaxy, the starburst ejecta in Model 2 must plow through a thicker layer of gas (with higher column density) before reaching the IGM. Thus more supernova energy is expending tun-

neling to the surface of the galaxy, leaving less energy to eject the enriched material. The higher column density also makes cooling more efficient in the swept up material, further reducing the energy available to expel enriched material. From Figures 5 and 7, we see that, by the end of the simulation, none of the enriched material has escaped beyond R_d , in stark contrast to Model 1. Also, from Table 2, we note that, although a slightly larger amount of unenriched gas is ejected, much less enriched material escapes the galaxy. This suggests that the location of a starburst or supernova can be an important factor in determining how the final products of stellar evolution are distributed.

3.3. Model 3

In Model 3 the energy input rate is identical to that of Model 1, but the supernovae occur over 80% of the galactic disk. This distribution represents the opposite extremum from Models 1 and 2. Whereas those models represent the results of starburst-like activity, Model 3 represents the situation of steady, self-regulated star formation throughout the disk.

The evolution of the density and tracer for Model 3a is shown in Figure 8. As can be seen in the figure, because the supernovae are spread out over a large fraction of the disk, they only interact with a few of their closest neighbors. The galactic gas, therefore, has a significant amount of time to relax between supernova events. The result is that most of the enriched material is retained by the galaxy as indicated in Figure 5. This is also supported by the very low ejection efficiencies of this model in Table 2. This model suggests that highly distributed star formation will be much less efficient at ejecting enriched material than more concentrated starbursts.

Because this model shows the least efficient ejection and is perhaps most subject to overcooling and weighting down due to the relatively high mass contained in each supernova (since few go off in previously evacuated regions), we also test a version of this model that enforces an maximum gas density ($\rho_{SN} < 10^{-26} \text{ g cm}^{-3}$) inside the supernova region for all events (Model 3b). This should tell us if the high mass inside the initial supernova region is responsible for the poor ejection efficiency. Instead, we find the evolution of this model to be very similar to Model 3a. Although Model 3b does show a slightly higher metal ejection efficiency ($\xi_Z = 0.24$), the difference would not seem to invalidate any of our results.

Model 3c is yet another variant of this basic model. Model 3c uses half the normal number of zones in each direction; it is intended to test the effect of resolution on our conclusions. We note that the low resolution model shows less efficient metal ejection ($\xi_Z = 0.17$) than the higher resolution equivalent. The lower ejection efficiency of Model 3c is most likely attributable to extra numerical diffusion of the ejecta into the surrounding galactic gas. However, the difference is not dramatic, suggesting that our results are well enough resolved to support our general conclusions.

3.4. Model 4

Model 4 is similar to Model 3, except that the supernovae are concentrated within the inner 30% of the disk. Thus it represents an intermediate case between Models 1

and 3. The evolution of the density and tracer for this model is shown in Figure 9. From Figure 5 we see that after 100 Myr, only a small amount of tracer has been lost beyond R_d , although the calculated metal ejection efficiency ($\xi_Z = 0.60$) is clearly higher than Model 3 but much less than Model 1. Thus, even a moderate distribution of supernova energy can significantly reduce the ejection efficiency of enriched gas.

Because the total supernova energy input in Models 3 and 4 is less than the binding energy of the gas, it might be argued that the supernovae have not had sufficient time to have a significant effect by the end of the simulations. In order to examine the possibility that continued supernova input may change our conclusions, we plot, in Figure 10, the time evolution of the internal and internal plus kinetic energies of Model 3. As can be seen, the energy of the model maintains an approximately steady-state, in which energy is radiated away at the same rate at which it is input by supernovae. We obtain very similar results for Model 4. These models would not, therefore, evolve significantly if the simulations were carried out for longer times.

3.5. Model 5

Model 5 is similar to Model 1 except that the energy input rate is increased by an order of magnitude. The supernova rate is therefore much closer to that of the Milky Way than in the previous models, as might be expected due to the similar surface density of gas and overall disk area of the models as compared to the Milky Way. The evolution of the density and tracer for this model is shown in Figure 11. Similar to Model 1, nearly all of the enriched material chimneys out of the galaxy along the symmetry axis, while at the same time, very little mass is lost from the remainder of the disk. Thus, our conclusion that highly concentrated starbursts result in efficient metal ejection without disturbing the bulk of the galaxy does not appear to be strongly dependent on the overall energy input rate.

3.6. Model 6

Model 6 has the same supernova rate as Model 5, yet the supernovae are spread over 80% of the disk, as in Model 3. The evolution of the density and tracer for this model is shown in Figure 12. In contrast with Model 3 (Figure 8), we see that the rate of energy input is sufficient to lead to some “tunneling,” providing low densities avenues for the loss of some enriched gas, particularly at small radii. Nevertheless, the loss of tracer for Model 6 is still small ($\xi_Z = 0.60$) compared to highly concentrated runs and there is very little supernova-driven mass loss by the end of the simulation ($\xi = 0.096$). However, we clearly see in Figure 10 that the energy input has not reached a steady state for this model. The energy input rate remains greater than the rate of loss due to radiative emission. If supernovae were to continue at the modeled rate indefinitely, the disk would eventually be destroyed, similar to what we observe in Model 7, discussed below. However, it is more realistic to assume that the supernova rate is correlated with the gas density in the disk, and thus the supernovae would likely shut off before that could happen, in which case the disk may remain intact.

3.7. Model 7

Model 7 is similar to Model 6 except that the energy input rate is increased by yet another order of magnitude. The evolution of the density and tracer for this model is shown in Figure 13. The supernova energy input rate of Model 7 greatly exceeds the radiative efficiency of the galaxy. The result, as can be seen in Figures 5, 6, and 13, is that after 70 Myr, nearly all of the tracer added to the galaxy so far is lost, and the disk itself is completely disrupted, leading to extensive mass loss. Since we have fixed the duration of the supernovae injection for this model at 100 Myr, the continuous infusion of enriched material ensures a residual of tracer elements are found even at late epochs (see Fig. 5). The results of this model suggest that, for supernovae distributed over a large fraction of the galaxy, a high efficiency of metal loss will be accompanied by significant overall mass loss.

3.8. Model 8

Model 8 is similar to Model 3 except that the mass of the galaxy is an order of magnitude smaller. This model allows us to explore the dependence of our results on galaxy mass. A greater loss of enriched gas relative to Model 3 is expected for two reasons. Firstly, the potential of Model 8 is significantly shallower than that of Model 3 (Figure 3). Secondly, while the two models have same supernova energy input rate, the total radiative emission rate of Model 8 is reduced by more than an order of magnitude relative to that of Model 3 (due to the lower overall gas mass and lower gas density).

The evolution of the density and tracer for Model 8 is shown in Figure 14. As can be seen, the system is unable to relax significantly between supernova events. The gas distribution therefore becomes highly disturbed, even more so than that of Model 6, despite the fact that these two models have the same energy input rate per unit gas mass. The difference is again due both to the shallower gravitational potential of Model 8 and its reduced radiative efficiency.

The evolution of the tracer for Model 8 shows three distinct behaviors. Initially, no tracer is lost to the system. After approximately 60 Myr, tracer begins to be lost at an approximately constant rate. Late in the simulation, the tracer abundance flattens, i.e. enriched material is lost to the system at roughly the same rate it is being added. As can be seen in Figure 14, the early losses of tracer are the result of material “chimneying” near the symmetry axis. The increase in the loss rate at approximately 85 Myr, occurs when enriched material also begins to expand beyond R_d in the equatorial plane of the disk (see the last frame of Figure 14).

4. DISCUSSION AND IMPLICATIONS

We have performed three-dimensional simulations of the evolution of enriched gas within dwarf disk galaxies. In these simulations, supernovae occur at random intervals and at random locations over prescribed fractions of the disk area. Our primary interest is to consider the efficiency of metal ejection for these systems, and its consequences for the evolution of dwarf galaxies, as we discuss below.

In general, we find that supernovae are less effective at ejecting enriched material from dwarf disk galaxies than

has been suggested in previous work. The key difference between the current and the earlier models (Mac Low & Ferrara 1999) is that the earlier studies triggered supernovae either within the cores of the galaxies, or elsewhere within the systems but still with very high local efficiency. In those models, representative of starbursts, the ambient gas was unable to relax between supernova events, and enriched gas could rapidly “chimney” out of the systems. This same behavior is seen in our starburst models (1, 2, and 5). In our remaining models, with supernovae distributed over 30 or 80% of the disk, a substantial fraction of the metals are retained. An important implication is that closed-box models for the chemical evolution of these galaxies may be more appropriate when supernovae are expected to be distributed throughout the disk than when they are concentrated in the central core or bulge region. Nevertheless, we find in all our models that a galactic outflow is set up in which at least some fraction of the available metals is ejected.

4.1. Comparison with Theoretical Supernova Rates

In the self-regulated star-formation model of Lin & Murray (1999), massive stars ionize and heat surrounding gas, preventing further star formation until the massive stars evolve off of the main sequence. This picture leads to a straightforward prediction for the formation rate of massive stars and the resulting supernova rate. From Lin & Murray (1999), the number of massive stars within a disk out to radius R is given approximately as

$$N_* \sim \frac{2\pi R^2 H}{\frac{4}{3}\pi R_S^3}, \quad (15)$$

where

$$H = 2^{1/2} c_s / \Omega \quad (16)$$

is the scale height of the gas, Ω is the rotational frequency at R ,

$$R_S^3 = \frac{Q_*}{\frac{4}{3}\pi n^2 \alpha_B} \quad (17)$$

is the Strömngren sphere radius, Q_* is the rate of emission of photoionizing photons by a massive star averaged over the population of massive stars, n is the average number density of the gas, and α_B is the case B recombination coefficient (Osterbrock 1989). Using reasonable values for the above parameters, it is found that

$$N_* \sim 2000 R_{10}^{-7/2} M_{10}^{5/2} b_{.1}^2, \quad (18)$$

where R_{10} is the radius of the disk in units of 10 kpc, M_{10} is the total mass of the system in units of $10^{10} M_\odot$, and $b_{.1}$ is the gas-to-total mass ratio, in units of 0.1. An L_* galaxy, such as the Milky Way today, is predicted to have supernova rates on the order of one per century, close to the observed rate.

For galaxies such as the one used for Models 1-7, supernova rates of $\sim 100 \text{ Myr}^{-1}$ would be expected, intermediate to the rates applied in Models 3 and 6. It might be expected, therefore, that the loss of enriched material for a galaxy of that mass undergoing self-regulated star formation would lie between 21% and 60%. We note, however, that the supernova rate would not remain at this value throughout the history of the galaxy. Rather, it would decrease as the square of the gas mass, assuming that the

gas scale height remained constant with time. The rate of enrichment would, therefore, decrease linearly with the gas fraction, as gas is converted into stars.

A galaxy such as that in Model 8 would be predicted to have a supernova rate $\sim 6 \text{ Myr}^{-1}$, several times less than applied in that model. Therefore, the loss of enriched material for such a galaxy undergoing self-regulated star formation may be significantly less than seen for Model 8 (53%).

4.2. Implications for Dwarf Galaxy Evolution

In the least massive galaxies (total masses $\lesssim 10^9 M_{\odot}$), simulations of both disk and spheroidal systems find that enriched gas from supernovae may be largely lost to the systems (Mac Low & Ferrara 1999; Sommer-Larsen, Götz, & Portinari 2003; Fragile et al. 2003). Such evolution is supported by observations which find poor self-enrichment efficiency in many low-mass systems (Mateo 1998; Grebel 2001; Harbeck et al. 2001; Prochaska et al. 2003).

In more massive systems, however, our current simulations find that the supernova rates expected for self-regulated star formation do not lead to significant loss of enriched gas when the supernovae are spread over a reasonable fraction of the disk. Such galaxies would, therefore, be expected to be efficiently self-enriched. Highly efficient loss of enriched gas occurs only if star formation occurs in concentrated bursts or significantly exceed estimated self-regulated rates. In those cases, the inability of the gas to relax between supernova events allows substantial loss.

Our conclusions apply primarily to the outputs of Type

II supernovae, the progenitors of which are massive, young stars. The short lifetimes of these objects do not allow for sufficient time to migrate large distances from their places of birth. Therefore, they are generally associated with regions of active star formation. In disk galaxies, these are near the midplanes, where the gas density is highest. The placement of the supernovae in the midplanes of our models is, therefore, a good representation to the actual distribution of Type II supernovae within galaxies. The progenitors of Type I supernovae, on the other hand, are older systems. Type I events may therefore occur further away from the disk midplane, giving them a better chance to eject enriched material from the galaxy. This is especially interesting, given that Type I supernovae are believed to be the dominant source of iron in galaxies, accounting for approximately 70% of the total production (Nomoto et al. 1984; Woosley et al. 1986; Woosley & Weaver 1986; Matteucci 1988). It is possible that although dwarf galaxies are able to retain the heavy elements produced by Type II events, they may still be depleted in iron. This picture is supported by two-dimensional numerical simulations of Type I and Type II supernovae (Recchi, Matteucci, & D’Ercole 2001).

This work was performed under the auspices of the U.S. Department of Energy by University of California, Lawrence Livermore National Laboratory under Contract W-7405-Eng-48. This work is partially supported by NASA through an astrophysical theory grant NAG5-12151.

REFERENCES

- Anninos, P., Fragile, P. C., & Murray, S. D. 2003, *ApJS*, 147, 177
 Blumenthal, G. R., Faber, S. M., Primack, J. R., & Rees, M. J. 1984, *Nature*, 311, 517
 Cole, S., Aragon-Salamanca, A., Frenk, C. S., Navarro, J. F., & Zepf, S. E. 1994, *MNRAS*, 271, 781
 Dekel, A., & Silk, J. 1986, *ApJ*, 303, 39
 De Young, D. S., & Gallagher, J. S. 1990, *ApJ*, 356, L15
 De Young, D. S., & Heckman, T. M. 1994, *ApJ*, 431, 598
 Dong, S., Lin, D. N. C., & Murray, S. D. 2003, *ApJ*, 596, 930
 Ferrara, A., & Tolstoy, E. 2000, *MNRAS*, 313, 291
 Fragile, P. C., Murray, S. D., Anninos, P., & Lin, D. N. C. 2003, *ApJ*, 590, 778
 Fragile, P. C., Murray, S. D., Anninos, P., & van Breugel, W. 2004, *ApJ*, 604, 74
 Freedman, W. L. et al. 2001, *ApJ*, 553, 47
 Gallagher, J. S. & Hunter, D. A. 1987, *AJ*, 94, 43
 Gibson, B. K., Maloney, P. R., & Sakai, S. 2000, *ApJ*, 530, L5
 Grebel, E. K. 2001, *ASSS*, 277, 231
 Harbeck, D., Grebel, E. K., Holtzmann, J., Guhathakurta, P., Brandner, W., Geisler, D., Sarajedini, A., Dolphin, A., Hurley-Keller, D., & Mateo, M. 2001, *AJ*, 122, 3092
 Katz, N., Weinberg, D. H., Hernquist, L., & Miralda-Escude, J. 1996, *ApJ*, 457, L57
 Kauffmann, G. 1996, *MNRAS*, 281, 475
 Kennicutt, R. C. 1989, *ApJ*, 344, 685
 Kennicutt, R. C. 1998, *ApJ*, 498, 541
 Klypin, A., Nolthenius, R., & Primack, J. 1997, *ApJ*, 474, 533
 Lin, D. N. C., & Murray, S. D. 1992, *ApJ*, 394, 523
 Lin, D. N. C., & Murray, S. D. 2000, *ApJ*, 540, 170
 Mac Low, M.-M., & Ferrara, A. 1999, *ApJ*, 513, 142
 Mateo, M. 1998, *ARA&A*, 36, 435
 Matteucci, F. 1988, in *Origin and Distribution of the Elements*, ed. G. J. Mathews, (Singapore: World Scientific), 186
 McCray, R. & Kafatos, M. 1987, *ApJ*, 317, 190
 McWilliam, A. 1997, *ARA&A*, 35, 503
 Navarro, J. F., Frenk, C. S., & White, S. D. M. 1997, *ApJ*, 490, 493
 Nomoto, K., Thielmann, F. K., & Yokoi, K. 1984, *ApJ*, 286, 644
 Osterbrock, D. E., 1989, *Astrophysics of Gaseous Nebulae and Active Galactic Nuclei* (University Science Books)
 Persic, M., Salucci, P., & Stel, F. 1996, *MNRAS*, 281, 27
 Prochaska, J. X., Gawiser, E., Wolfe, A. E., Castro, S., & Djorgowski, S. G. 2003, *ApJ*, 595, L9
 Quinn, T., Katz, N., & Efstathiou, G. 1996, *MNRAS*, 287, 49
 Recchi, S., Matteucci, F., & D’Ercole, A. 2001, *MNRAS*, 322, 800
 Silich, S. & Tenorio-Tagle, G. 1998, *MNRAS*, 299, 249
 Silich, S. & Tenorio-Tagle, G. 2001, *ApJ*, 552, 91
 Sommer-Larsen, J., Gelato, S., & Vedel, H. 1999, *ApJ*, 519, 501
 Sommer-Larsen, J., Götz, M., & Portinari, L. 2003, *ApJ*, 596, 47
 Stothers, R. 1972, *ApJ*, 175, 431
 Tegmark, M., Silk, J., Rees, M. J., Blanchard, A., Abel, T. & Palla, F. 1987, *ApJ*, 474, 1
 Weinberg, D. H., Hernquist, L., & Katz, N. 1997, *ApJ*, 477, 8
 White, S. D. M., & Rees, M. J. 1978, *MNRAS*, 183, 341
 Williams, L. L. R. & Saha, P. 2000, *AJ*, 119, 439
 Wolfe, A. E., Prochaska, J. X., & Gawiser, E. 2003, *ApJ*, 593, 215
 Woosley, S. E., Taam, R. E., & Weaver, T. A. 1986, *ApJ*, 301, 601
 Woosley, S. E. & Weaver, T. A. 1986, in *Radiation Hydrodynamics in Stars and Compact Objects*, eds. D. Mihalas, & K.-H. A. Winkler, (Berlin: Springer-Verlag), 91

TABLE 1
MODEL GALAXY PARAMETERS

Model	M_g (M_\odot)	Energy input rate (10^{51} erg Myr $^{-1}$)	Energy/event (10^{51} erg)	R_{SN}/R_d	SN input phase (Myr)	Simulation stop (Myr)
1	10^9	30	1	0.0	50	100
2	10^9	30	1	0.0 ^a	50	100
3	10^9	30	10	0.8	100	100
4	10^9	30	10	0.3	100	100
5	10^9	300	10	0.0	50	50
6	10^9	300	10	0.8	75	75
7	10^9	3000	1	0.8	100	100
8	10^8	30	10	0.8	100	100

^aOffset from center by $R_d/2$.

TABLE 2
GAS AND METAL EJECTION EFFICIENCIES

Model	ξ	ξ_Z
1	0.023	0.91
2	0.032	0.47
3a	0.027	0.21
3b ^a	0.027	0.24
3c ^b	0.027	0.17
4	0.028	0.60
5	0.016	0.99
6	0.096	0.60
7	0.98	0.99
8	0.064	0.53

^aDensity ceiling enforced on all supernovae.

^b $128 \times 128 \times 64$ resolution.

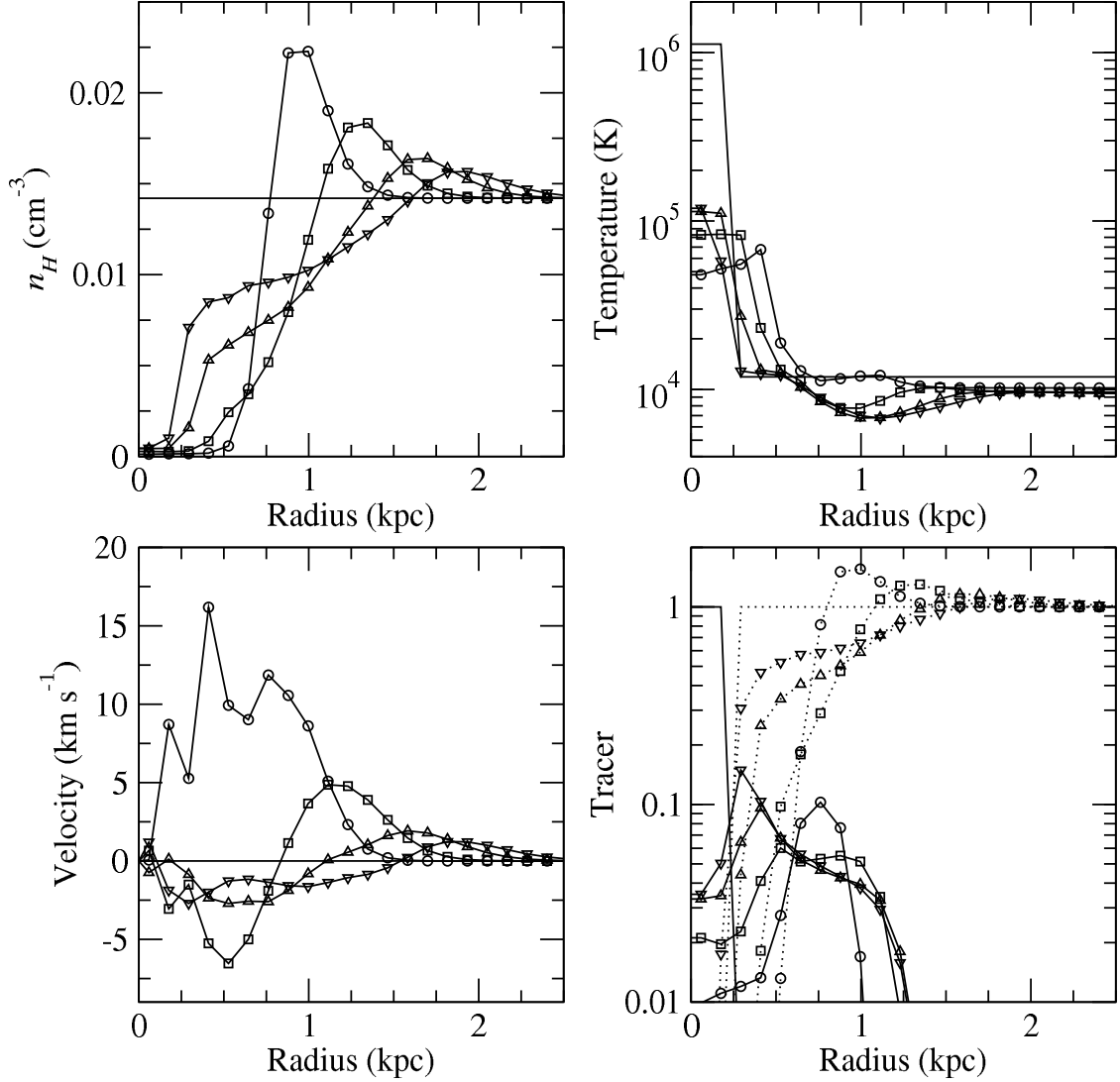


FIG. 1.— Density, temperature, velocity, and tracer distribution of a single supernova event in a homogeneous background. The data are from $t = 0, 25$ (circles), 50 (squares), 75 (triangles), and 100 (inverted triangles) Myr. The tracer plot tracks both enriched material (solid lines) and background gas (dotted lines).

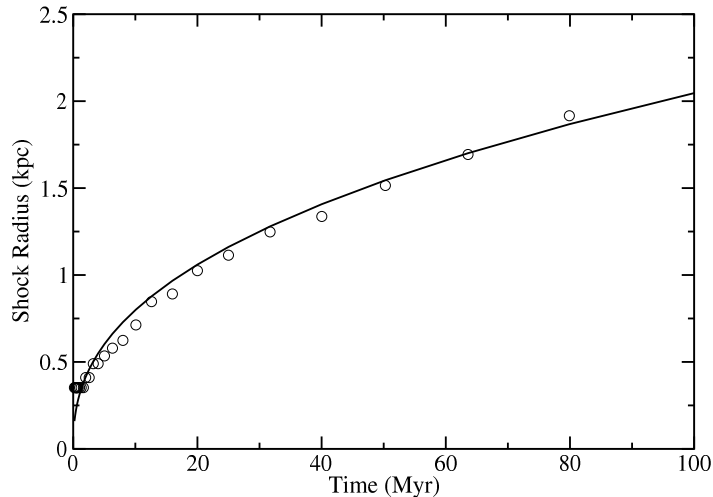


FIG. 2.— Shock radius as a function of time for a single supernova event in a homogeneous background. The data (circles) are best fit with a power-law of the form $r_{sh} \propto t^{0.41}$ (solid curve), close to the Sedov-Taylor solution.

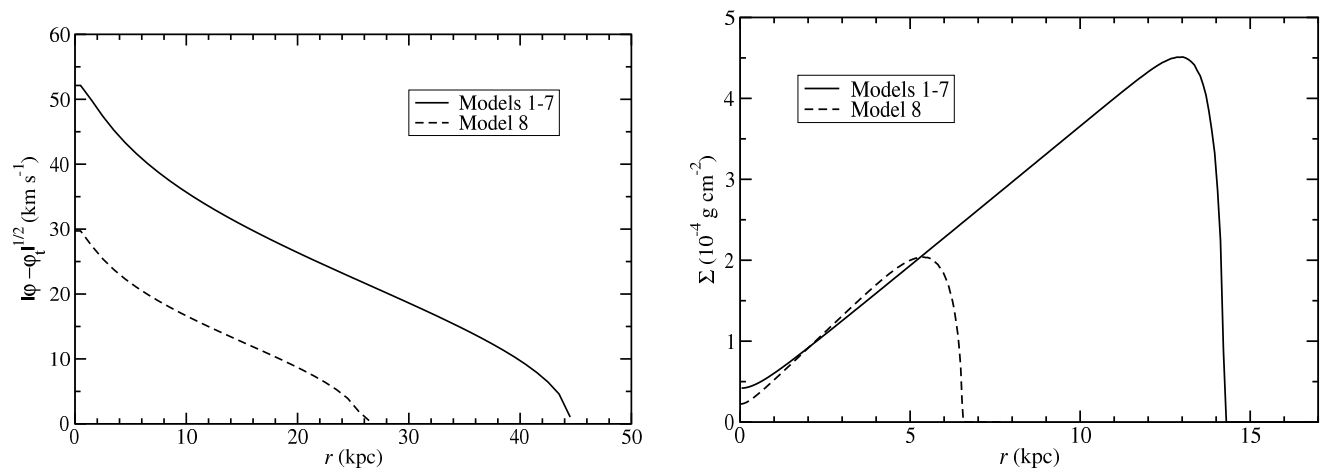


FIG. 3.— (a) Square root of the absolute value of the normalized gravitational potential as a function of radius; (b) integrated column density as a function of radius in the midplane of the disk for the galaxies in Models 1-7 (solid curves) and Model 8 (dashed curves).

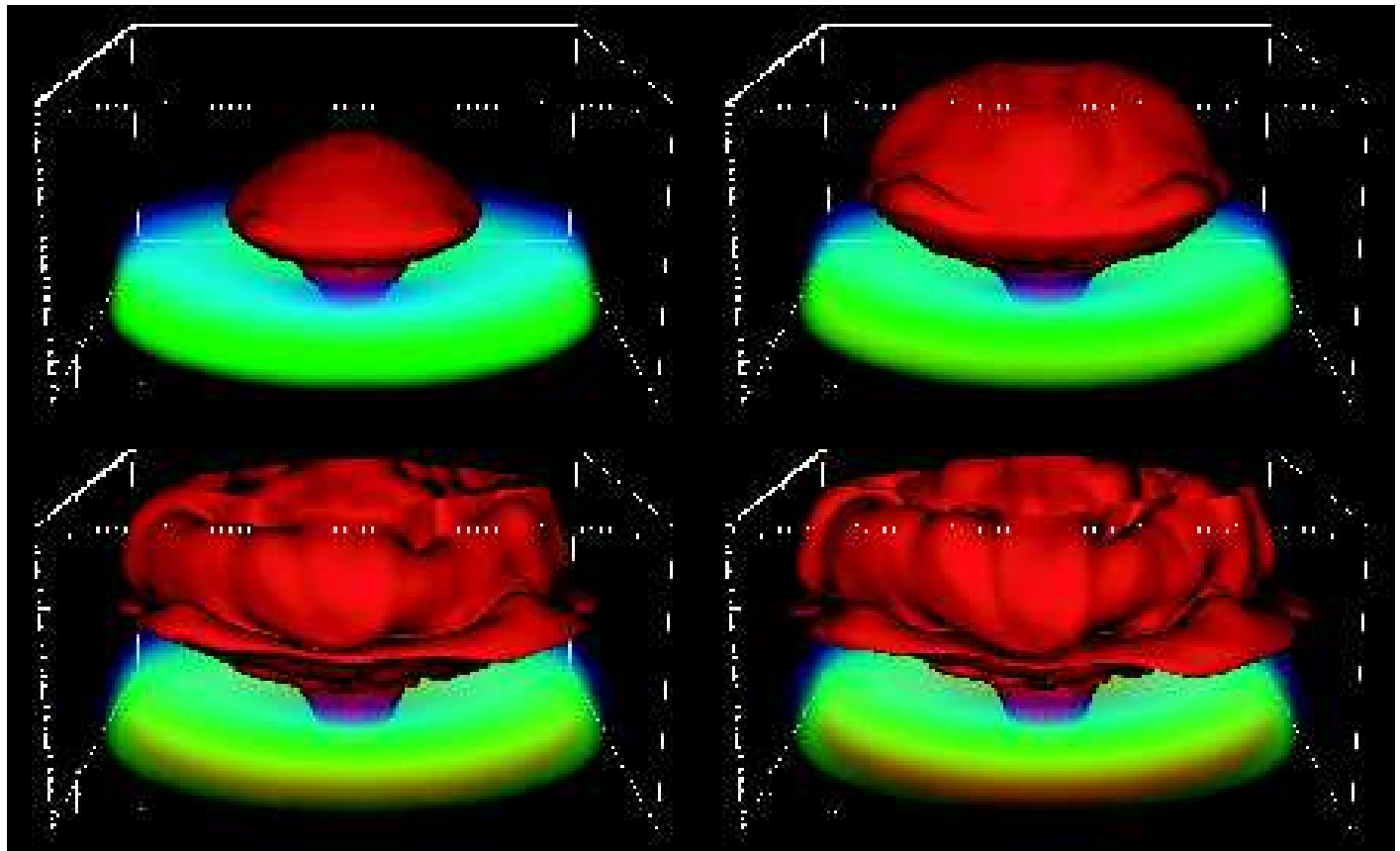


FIG. 4.— Volume rendering of gas density plus an isosurface (in red) of metal tracer for Model 1 at $t = 25, 50, 75,$ and 100 Myr. The metal tracer surface is set at 0.1% of the input level. The box is $30 \times 30 \times 15 \text{ kpc}^3$; the major tick marks are spaced 4.5 kpc apart in the x - and y -directions and 2.25 kpc apart in the z -direction.

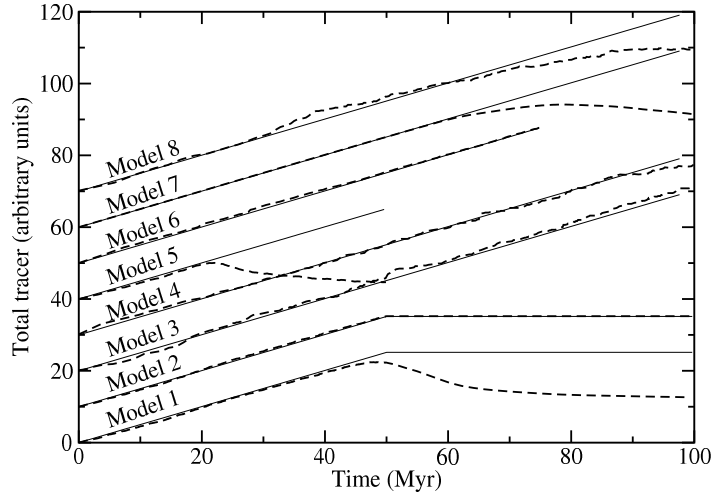


FIG. 5.— Plot of total tracer contained within R_d as a function of time for all models. The data are adjusted to have the same slope and then offset to make the plot more legible. The thin solid lines are provided as a guide of the average tracer input rate for each model. Note that, for Models 1 and 2, supernova input ends after 50 Myr. The remaining models have continuous supernova input for the duration of the simulations.

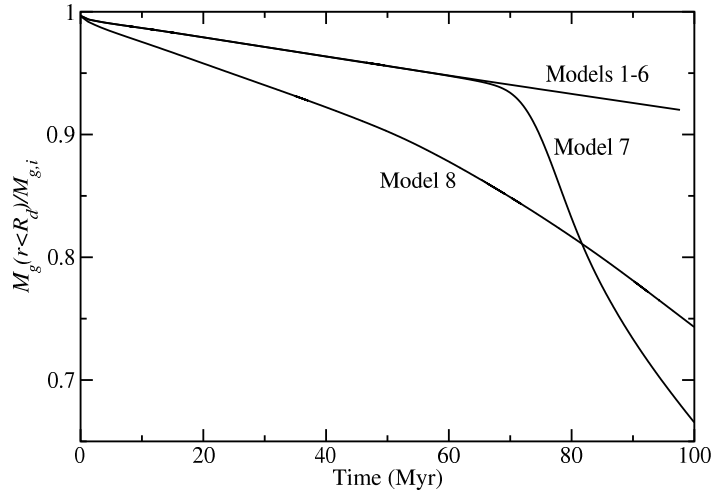


FIG. 6.— Plot of total gas mass (M_g) contained within R_d as a function of time for all models. The data are normalized to the initial gas mass of each galaxy. Note that some mass escapes beyond R_d simply because the galaxies are not in initial pressure equilibrium with the background at the cut-off radius. This accounts for virtually all of the loss for Models 1-6 and the early loss in Models 7 and 8. Only Models 7 and 8 show a deviation due to the energy input of supernovae at late time ($t \gtrsim 50$ Myr).

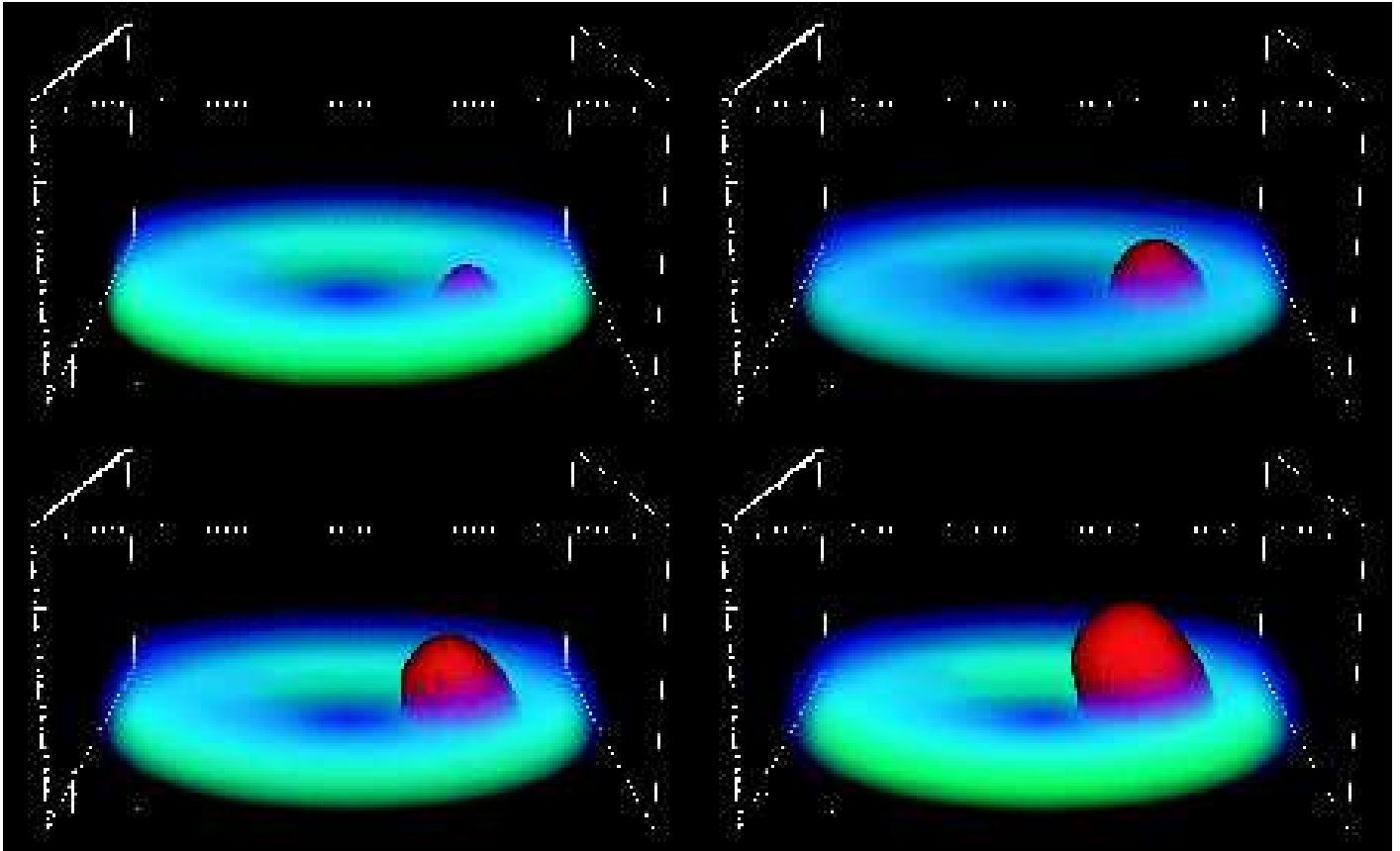


FIG. 7.— Same as Figure 4 for Model 2 at $t = 25, 50, 75,$ and 100 Myr.

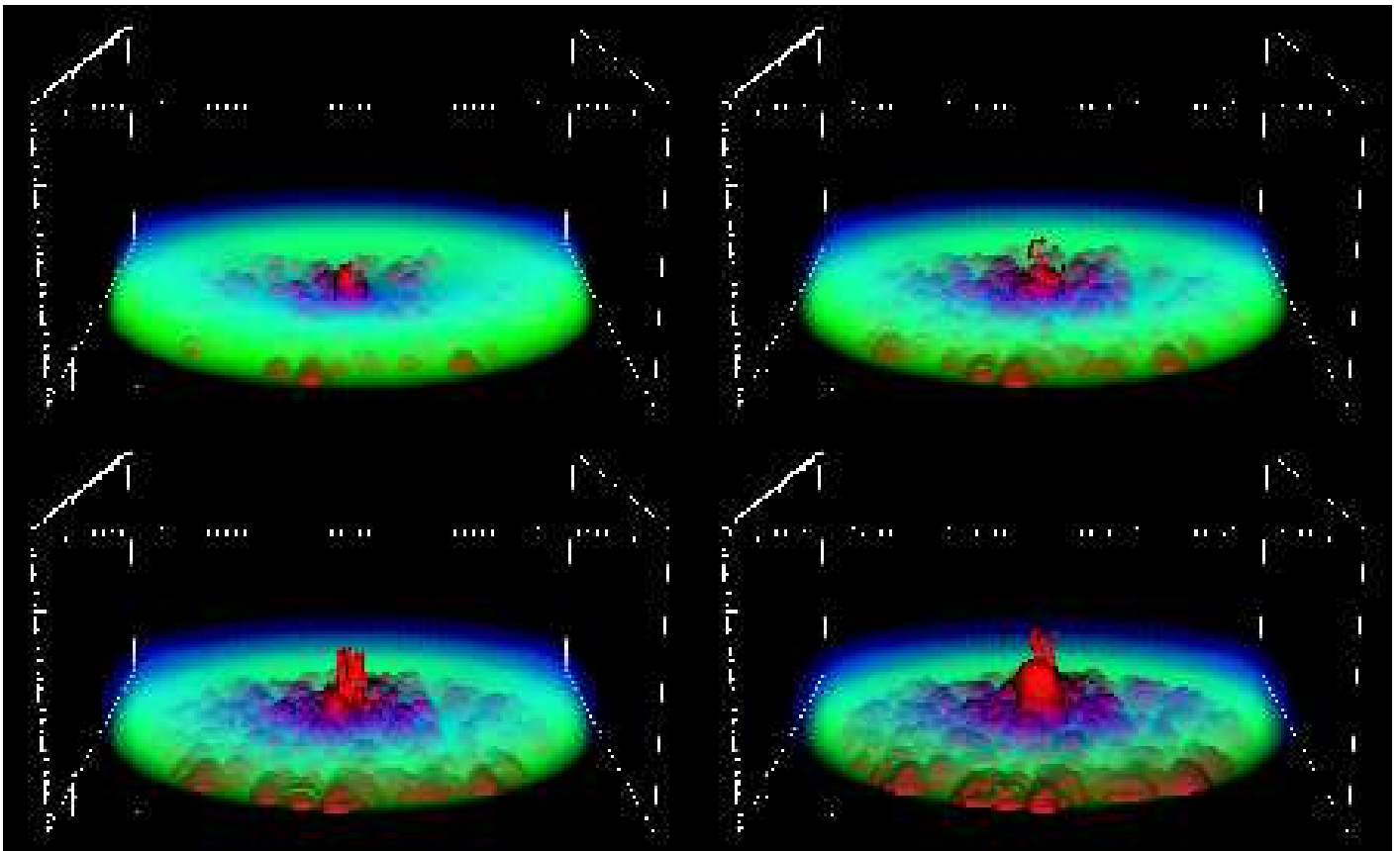


FIG. 8.— Same as Figure 4 for Model 3a at $t = 25, 50, 75,$ and 100 Myr.

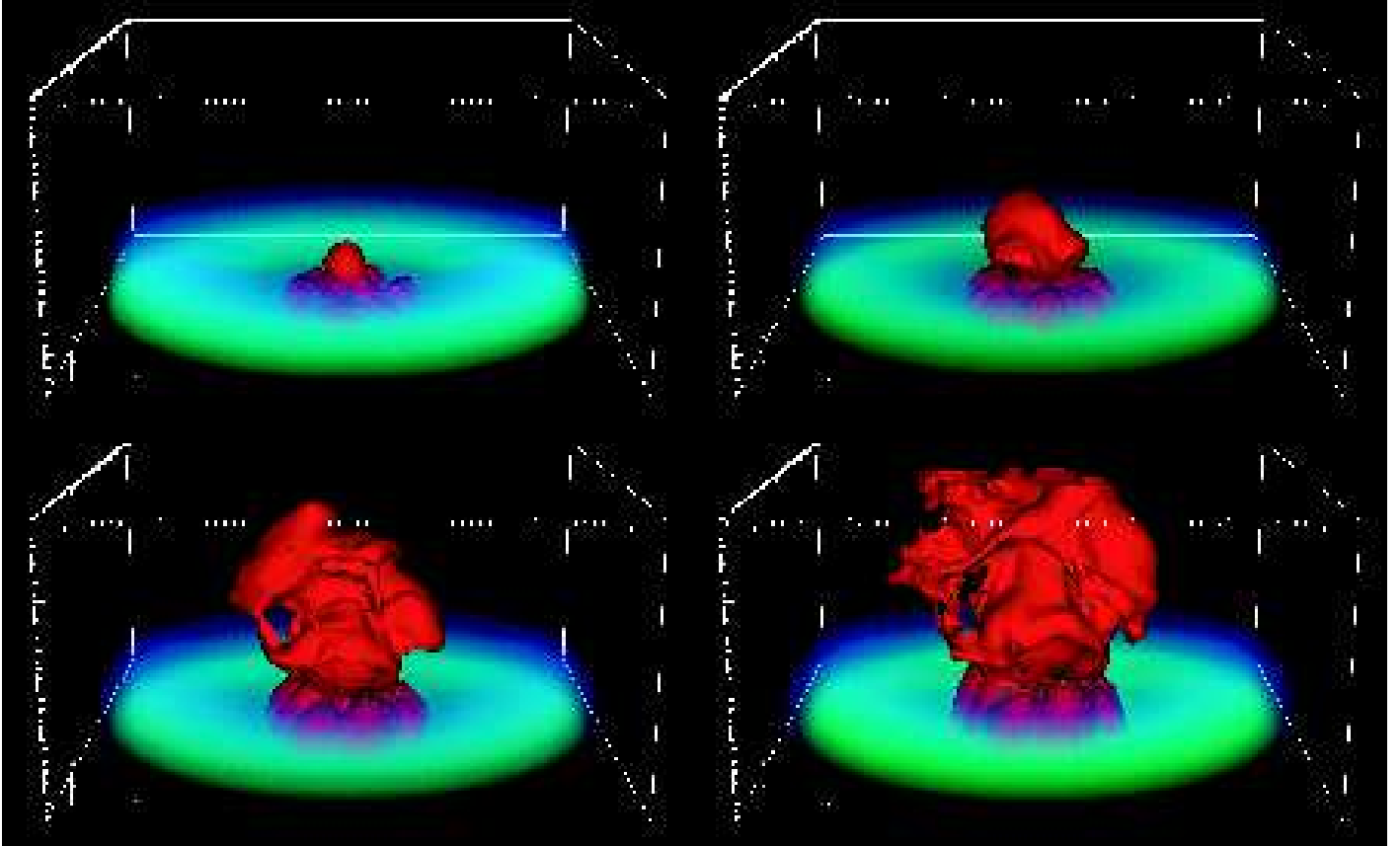


FIG. 9.— Same as Figure 4 for Model 4 at $t = 25, 50, 75,$ and 100 Myr.

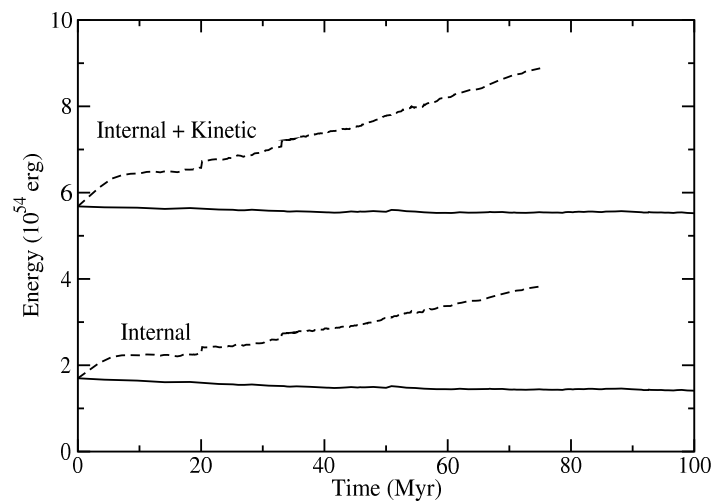


FIG. 10.— Internal and internal+kinetic energy as a function of time for Models 3 (*solid line*) and 6 (*dashed line*).

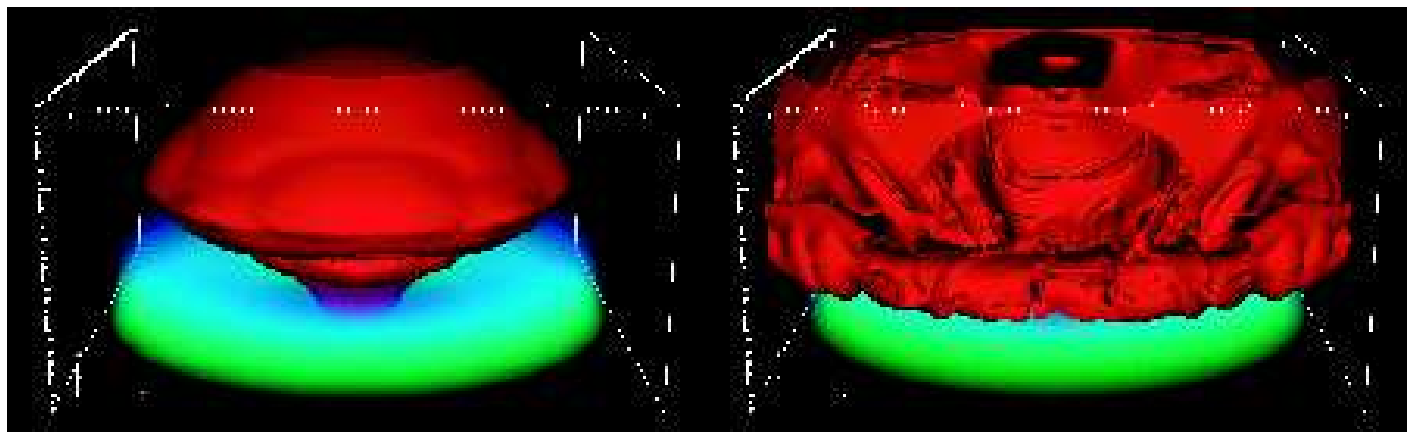


FIG. 11.— Same as Figure 4 for Model 5 at $t = 25$ and 50 Myr.

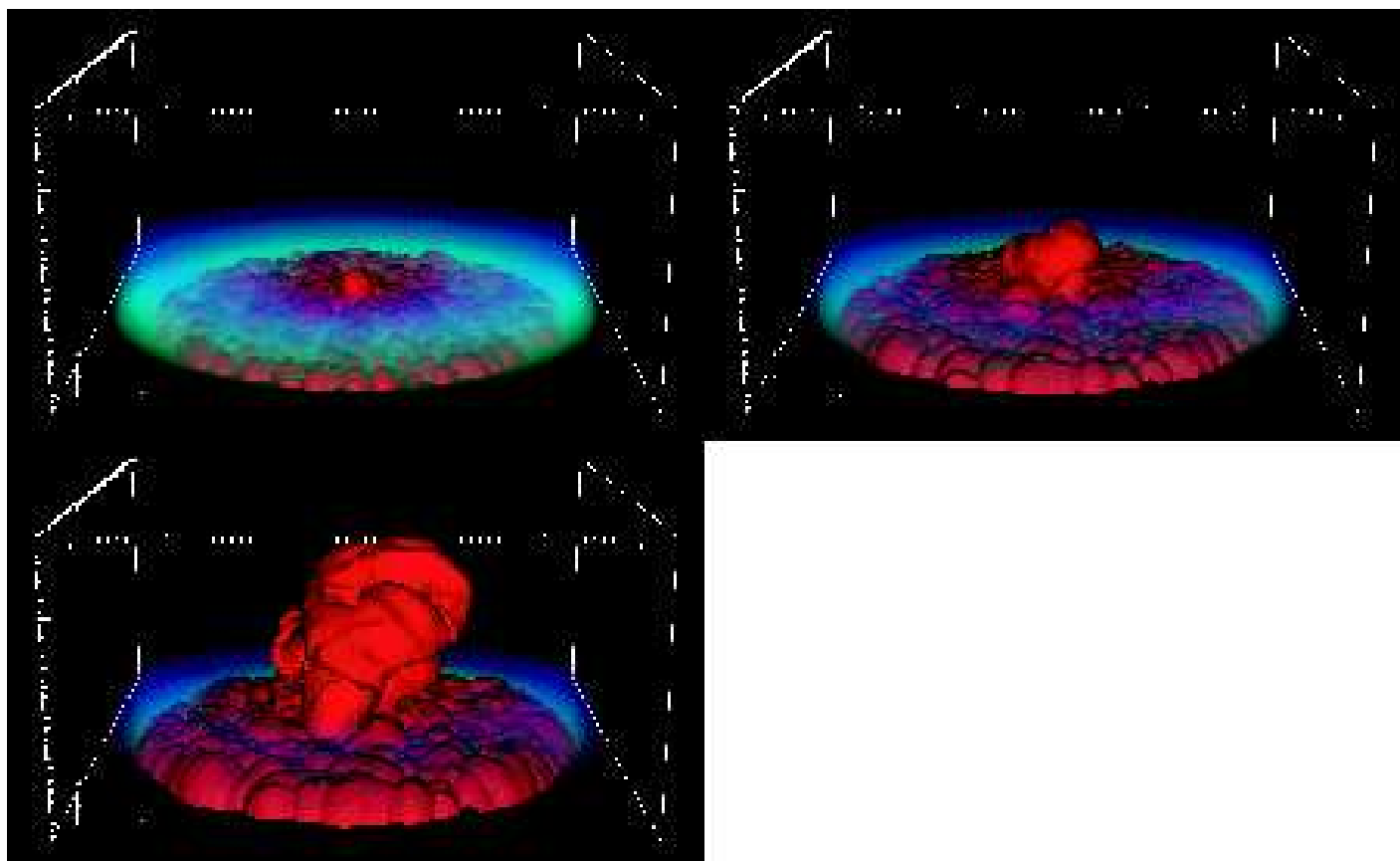


FIG. 12.— Same as Figure 4 for Model 6 at $t = 25$, 50, and 75 Myr.

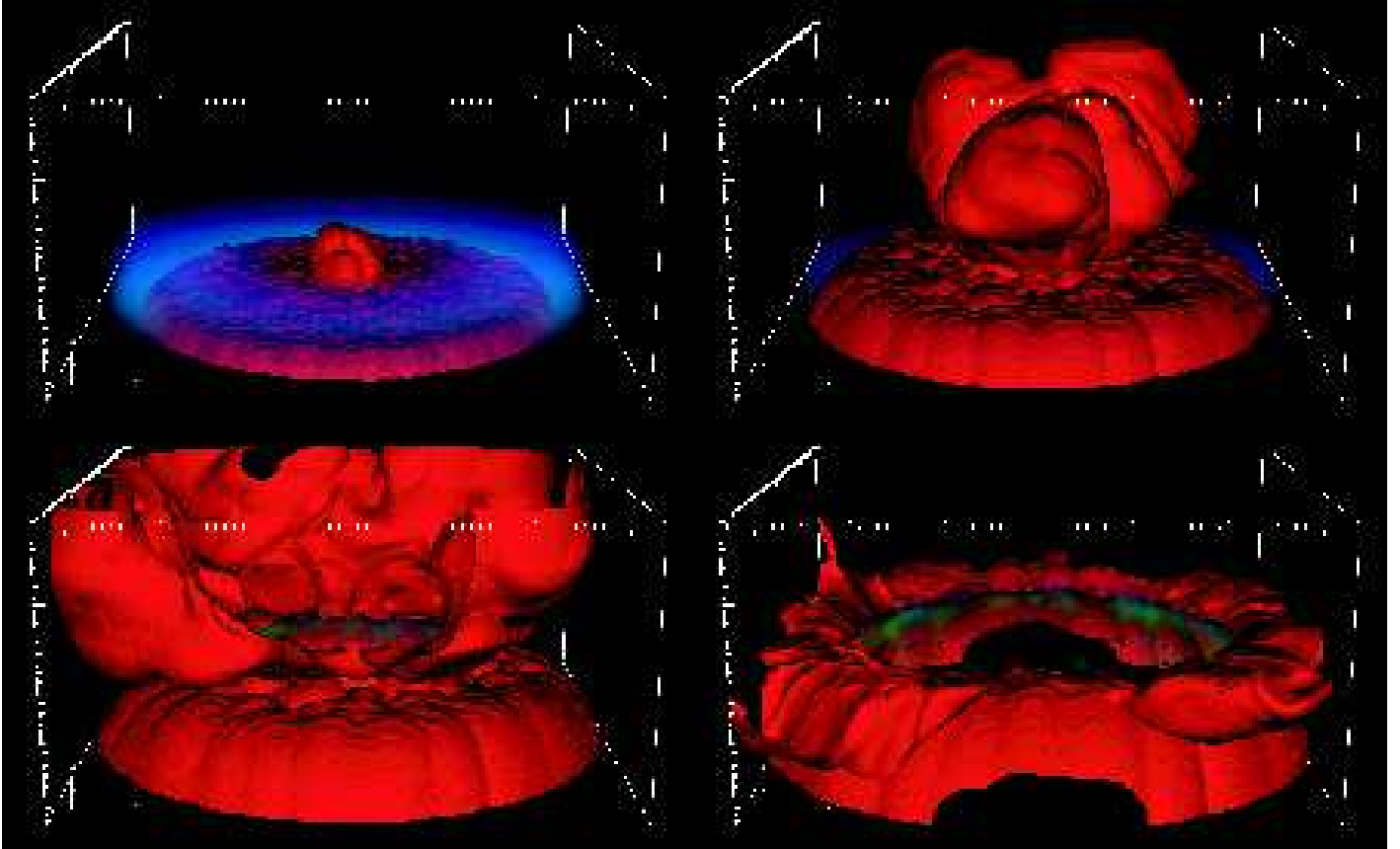


FIG. 13.— Same as Figure 4 for Model 7 at $t = 25, 50, 75,$ and 100 Myr.

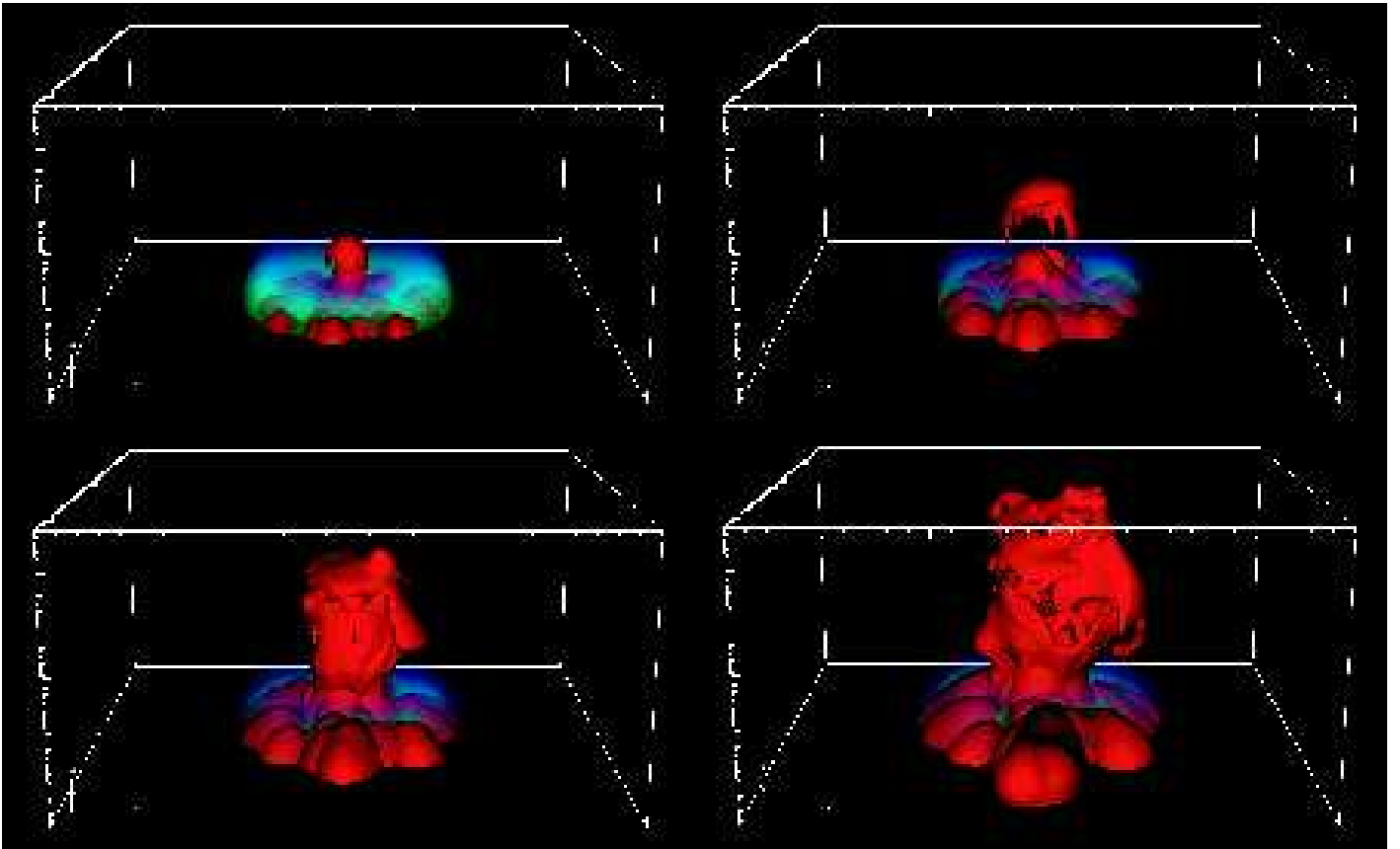


FIG. 14.— Same as Figure 4 for Model 8 at $t = 25, 50, 75,$ and 100 Myr.